scientific reports

Check for updates

OPEN

Coherent control of dark and bright spatio-temporal solitons of SPPs at a silver silica nano-composite interface with gain-assisted atomic medium

Naseem Elahi[1], Muhammad Ikram[1]✉, Najm Uddin[2], Latif Ur Rahman[3]✉, Nahid Fatima[4], Kamal Shah[4] & Thabet Abdeljawad[4,5,6]✉

This article investigates the coherent control of spatio-temporal bright and dark soliton pulses along with the associated intensity of surface plasmon polariton (SPP) waves at the interface of silver-silica nano-composite materials and a gain-assisted medium. A considerable control over SPPs soliton pulses is revealed by varying the position, time, and characteristics of the applied driving fields. The strength of solitonic pulses can vary based on system factors, potentially increasing, decreasing, or remaining constant over time. Periodic dark and bright solitons are also observed, with intensity patterns exhibiting exponential decay over time. When dispersion and nonlinearity are compared, stable solitons may maintain a constant intensity level of 60%. Moreover, the strength of surface plasmon polaritons (SPPs) can be adjusted between 0 and 100%. This adjustment is achieved by modifying external fields, allowing for either complete enhancement or total suppression of the SPPs. These findings provide a solid foundation for the development of active, compact, and fast photonic devices. They bridge the gap between light-matter interactions at the quantum level and the advancement of integrated nano-photonic devices. Such devices encompass applications in nano-scale sensing, logic gates, electrochemical sensing, optical switching, and biomedical imaging.

Keywords Surface plasmon polaritons, Density matrix formalism, Atomic coherence, Spatio-temporal soliton

A soliton is a localized and stable wave packet that occurs in nonlinear systems and maintains its shape owing to its self-strengthening characteristics. It is defined as any localized and stable solution of a nonlinear differential equation. Self-preserving wave packets manifest in several physical systems and phenomena[1]. Solitons demonstrate characteristics similar to particles, and have been thoroughly examined in Bose-Einstein condensates[2], nonlinear optical media[3], and field theories[4]. They may engage with one another either by annihilating, merging, or experiencing particle-like interactions such as repulsion, attraction, or collision[5]. Vector solitons are a specific type of solitons that travel through a medium with the same group velocity and have several interlinked components. The interactions of bound vector solitons and soliton complexes have been investigated by coupled nonlinear Schr dinger equations[6,7]. Cross-phase modulation assists in trapping soliton and the creation of vector solitons, which are beneficial for optical switching and in simulating gravitational-like phenomena in optics[8]. Solitons have importance in both theoretical and practical domains. Mathematics offers essential insights into nonlinear differential equations, symmetries characterized by Lie groups and algebras, and their applications in differential and algebraic geometry. Solitons play a key role in contemporary communication systems, facilitating efficient data transmission[9], facilitating long-distance digital signal transmission[10], and improving high-speed optical routing and advanced communication technologies[11]. Solitons endure in

[1]Department of Physics, Hazara University Mansehra, Mansehra 21300, Pakistan. [2]Government Ghazi Umara Khan Degree College , Lower Dir, KPK 18600, Pakistan. [3]Government College of Technology Mingora, Swat, KPK 19130, Pakistan. [4]Department of Mathematics and Sciences, Prince Sultan University, 11586 Riyadh, Saudi Arabia. [5]Department of Fundamental Sciences, Faculty of Engineering and Architecture, Istanbul Gelisim University,Avcilar, 34310 Istanbul, Turkey. [6]Department of Medical Research, China Medical University, 40402 Taichung, Taiwan. ✉email: mikphysics@gmail.com; Latifoptics1@gmail.com; tabdeljawad@psu.edu.sa

gathering substantial theoretical and experimental attention due to their wide applications in quantum and nonlinear systems. Zhang et al.[12] demonstrated the creation of vector solitons by four-wave mixing between two polarization components in passively mode-locked fiber lasers. Yang[13], attained substantial improvements in the analysis of results to non-integrable nonlinear Schr dinger equations, while Kaup[14], inspected the interior dynamics of vector solitons in nonlinear optical fibers. Dumitru et al.[15], examined the firmness of moving vector solitons controlled by connected nonlinear Schr dinger systems. Stone et al.[16], explored complicated soliton interactions in graphene-based mode-locked fiber lasers, whereas Lu et al.[17], recognized soliton fission in isotropic nonlinear media. Hani et al.[18], investigated polarization effects on the creation of vector solitons in erbium-doped fiber lasers using carbon nano-tube mode-locking. On the theoretical side, Ye et al.[19] applied the Darboux transformation to obtain dark vector soliton solutions of the modified Korteweg de Vries equation. Zhu et al.[20] examined the influence of fourth-order dispersion on vector solitons in weakly birefringent fibers, while Ding et al.[21] classified degenerate and non-degenerate vector solitons based on distinct wavenumber configurations. Xu et al.[22] studied dark bright vector solitons in spin orbit-coupled Bose Einstein condensates, and Tang et al.[23] explored various soliton types including bright-dipole, tripole, dark bright, and valley-Hall edge solitons in super-honeycomb lattice structures. Djazet et al.[24] proposed stability criteria for dissipative vector solitons, and Huang et al.[25] investigated quantum squeezing in vector slow-light solitons within coherently driven atomic media. Complementary studies on scalar solitons are reported in Refs.[26–31], while the interplay between nonlinear polarization states and cavity solitons in Kerr resonators has been extensively explored[32–34]. Some of the problems are solved mathematically in the regime of a coupled non-linear differential equation systems[35–37]. Recent works also reveal the coexistence and mutual interaction of dark vector soliton Kerr combs and polarization-dependent nonlinear states[38,39].

Surface plasmon polariton (SPP) waves are non-radiative electromagnetic excitations resulting from the coupling of light with collective electron oscillations at a metal dielectric interface[40–42]. These waves propagate along the interface until dissipated by losses. When light excites surface plasmons, the associated refractive-index change can be detected using surface plasmon resonance (SPR) sensors[43]. Surface Plasmon Polaritons have significantly influenced advances in plasmonics, optics, and photonics[44–47], with so many applications like terahertz technology[48], drugs[49], sensing and imaging[50,51], optical logic gates[52], and nano-scale switching[53]. Advanced sensing platforms employing plasmonics include bio-sensors[54], gas detectors[55], DNA sensors[56], temperature sensors[57], and electrochemical detectors[58,59]. However, high propagation losses remain a key limitation. To overcome this, hybrid and composite plasmonic waveguides have been developed to enhance performance and reduce dissipation[60]. Saeed Asgarnezhad and colleagues theoretically explored surface polaritonic dynamics in various metamaterial atomic systems. They proposed coupler-free and reconfigurable waveguides enabling controlled excitation and propagation of rogue waves, breathers, and frequency combs through electromagnetically induced transparency. Their studies also demonstrated stable linear and nonlinear surface polariton propagation with active Raman gain, field enhancement, group velocity control, and enhanced Kerr nonlinearity at dielectric metamaterial interfaces[61–64]

In this work, we investigate the coherent control of spatio-temporal bright and dark soliton pulses and their corresponding SPP intensity modulation at the interface between a silver silica nano-composite and a gain-assisted atomic medium. The results show that bright and dark SPP solitons can be precisely tuned in both space and time by adjusting the driving-field parameters. Depending on the configuration, soliton intensity may increase, decay, or remain stable. Periodic bright and dark soliton patterns are also observed. By precisely manipulating the phase, amplitude, and temporal characteristics of optical fields at the nano-scale, such control enables tunable bright and dark SPP solitons, which are capable of sub-wavelength light confinement and ultra-fast response dynamics. These findings offer potential applications in optical communication, switching, and nonlinear nano-photonic systems

Model and equations

This study focuses on the interaction between silver-silica nano-composites and a gain-assisted atomic system arranged in an N-type four-level configuration, as shown in Fig. 1. In this configuration, the lowest energy state $|4\rangle$ is linked to the excited state $|1\rangle$ through a pump field E_1, characterized by the Rabi frequency R_1. Additionally, the intermediate state $|3\rangle$ interacts with the two higher energy states $|1\rangle$ and $|2\rangle$ via a probe field E_p, and a control field E_c, corresponding to the Rabi frequencies R_p and R_c, respectively. The frequency detuning of the pump and probe fields are defined relative to the atomic transition resonance frequencies, such that $\Delta_p = \omega_{13} - \nu_p$ and $\Delta_1 = \omega_{14} - \nu_1$. To analyze the system and derive its time-evolution equations, we employ the Hamiltonian under the dipole approximation and within the framework of the rotating wave approximation (RWA). The total Hamiltonian is expressed as $H = H_0 + H_I$, where H_0 represents the unperturbed (self-energy) component of the Hamiltonian, given by

$$H_0 = \hbar\omega_1 |1\rangle \langle 1| + \hbar\omega_2 |2\rangle \langle 2| + \hbar\omega_3 |3\rangle \langle 3| + \hbar\omega_4 |4\rangle \langle 4| \tag{1}$$

The Hamiltonian in the interaction picture, H_I, is expressed as:

$$H_I = -\frac{\hbar}{2} R_1 e^{-i\Delta_1 t} |4\rangle \langle 1| - \frac{\hbar}{2} R_p e^{-i\Delta_p t} |3\rangle \langle 1| - \frac{\hbar}{2} R_c |3\rangle \langle 2| + H \cdot c \tag{2}$$

The following is the master equation that is used to solve a system's dynamics at room temperature[65]:

$$\dot{\rho} = -\frac{i}{\hbar} [H_I, \rho] - \sum \frac{1}{2} \gamma \left(\kappa^\dagger \kappa \rho + \rho \kappa^\dagger \kappa - 2\kappa \rho \kappa^\dagger \right) \tag{3}$$

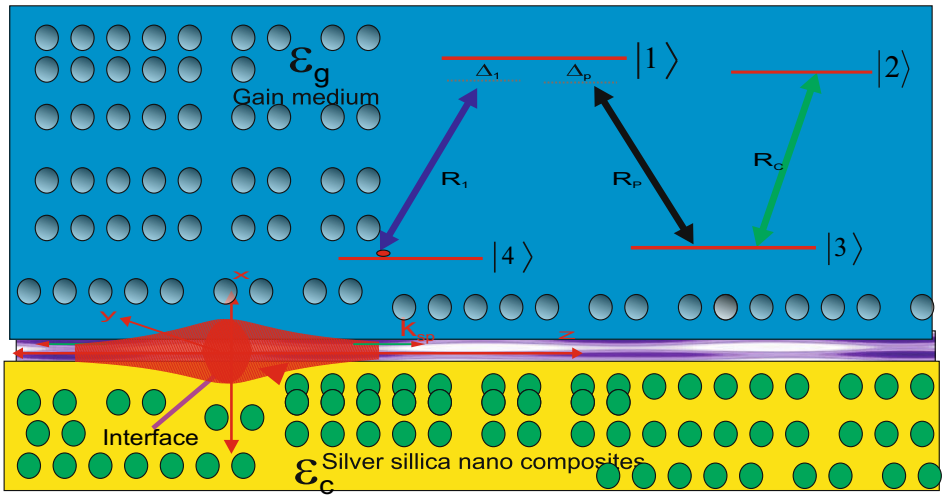

Fig. 1. Scheme for an N-type rotating gain assisted atomic configuration.

where the operators $\kappa^{\dagger}$ and κ are raising and lowering. The following is the atomic coherence of the probe field as determined by the second order $[\rho_{13}^{(2)}]$.

$$\rho_{13}^{(2)} = -i\left[\frac{4R_1^2\left(4\left(\gamma_{12}-i\Delta_p\right)\left(\gamma_{24}+\Delta_p-\Delta_1\right)-iR_c^2\right)}{\left(-i\gamma_{14}+\Delta_1\right)\left(4(i\gamma_{12}\Delta_p)\left(i\gamma_{13}\Delta_p\right)-R_c^2\right)A_2}+\frac{8\gamma_{14}\left(i\gamma_{12}+\Delta_p\right)R_1^2}{\left(\gamma_{13}+\gamma_{14}\right)\left(\gamma_{14}^2+\Delta_1^2\right)\left[4A_1+iR_c^2\right]}\right] \tag{4}$$

The contraction of the equation of motion involves making internal assumptions such as:

$$A_1 = \left(\gamma_{13}-i\Delta_p\right)\left(i\gamma_{12}+\Delta_p\right)$$
$$A_2 = 4\left(i\gamma_{24}+\Delta_p-\Delta_1\right)\left(-i\gamma_{43}-\Delta_p+\Delta_1\right)+R_c^2$$

For this Gain-assisted media, the computed susceptibility is expressed as follows[66]:

$$\chi = \frac{2N_0\varrho_{13}^2}{\epsilon_0\hbar R_p}\rho_{13}^{(2)} \tag{5}$$

where N_0 is the atomic number density and ϱ_{13} is dipole matrix element which shows transition between the atomic states.

$$\varrho_{13} = \sqrt{\frac{3\gamma_{13}\hbar\epsilon_0\lambda^3}{8\pi^2}} \tag{6}$$

The assisted mediums dielectric function interacted with the field is given by

$$\varepsilon_a = 1+4\pi\chi \tag{7}$$

The nano-composite materials dielectric function is formulated[67] as:

$$\varepsilon_c = \left[1+\frac{f_m\left(\varepsilon_{Ag}-\varepsilon_d\right)}{\varepsilon_d+\frac{1}{3}\left(1-f_m\right)\left(\varepsilon_Ag-\varepsilon_d\right)}\right]\varepsilon_d \tag{8}$$

In the composite material, f_m represents the volume fraction of silver nano-particles and ranges from $0 < f_m < 1$ corresponding to pure dielectric and pure metal. The dielectric function for silver is given[67] by:

$$\varepsilon_{Ag} = \varepsilon_\infty - \frac{(\omega_p)^2}{\omega^2+i\gamma_s\omega} \tag{9}$$

In this context, ω_p, γ_s, and ε_∞ represent the plasma frequency or collective oscillation frequency, scattering rate (accounting for energy losses due to collisions), and lattice contribution, respectively. The dispersion relation for SPPs under complex conductivity is given by[65]:

$$k_{sp} = \frac{2\pi}{\lambda}\sqrt{\frac{\varepsilon_a\varepsilon_c}{\varepsilon_a+\varepsilon_c}} \tag{10}$$

Parameters such as velocity, damping, wavelength, energy, propagation and penetration lengths, and propagation modes define the dispersion relation of SPPs. The propagation length, denoted by L_x, is defined by $L_x = \frac{1}{2\,\mathrm{Im}(k_{sp})}$. The SPP intensity decreases exponentially with propagation length, given by $e^{-2k_{sp}L_{sp}}$. This length indicates the distance along the interface where the SPP intensity is reduced to $1/e$ of its original value. The refractive and group indices of SPPs are given by:

$$n_{sp} = \sqrt{\frac{\varepsilon_a \varepsilon_c}{\varepsilon_a + \varepsilon_c}} \tag{11}$$

$$n_g^{sp} = \sqrt{\frac{\varepsilon_a \varepsilon_c}{\varepsilon_a + \varepsilon_c}} + \omega \frac{\partial}{\partial \Delta_p} \left(\sqrt{\frac{\varepsilon_a \varepsilon_c}{\varepsilon_a + \varepsilon_c}} \right) \tag{12}$$

The group velocity is given by $c/n^{sp}g$, and the propagation time is expressed as Lsp/v_g^{sp}. To incorporate Kerr nonlinearity into SPP propagation, the refractive index of SPPs is expanded as follows[68]:

$$n_{sp}^k = n_{sp}^{(0)} + I \frac{\partial n_{sp}}{\partial I}|_{I=0} \tag{13}$$

where $I = |\Omega_c|^2$ and $n_{sp}^{(0)}$ is refractive index without I or Kerr field Ω_c. The self Kerr nonlinearity is generated by third order of susceptibility, while cross Kerr nonlinearity is generated by the above method of Eq. (13). The envelope of the SPPs soliton pulse wave packet is given by[65]:

$$S_{sp}(z,t) = \exp(i(\omega t - kz))\xi(z,t) \tag{14}$$

where

$$\xi(z,t) = \xi_0 Sech\left[\gamma\left(t - \frac{z}{v_g^{sp}}\right)\right] \exp(igz) \tag{15}$$

where $\xi_0 = \sqrt{g/\Gamma}$ indicate the pulse amplitude and $Sech[\gamma(t - \frac{z}{v_g^{sp}})]$ is the function of hyperbolic secant shows the shape of the pulse. In addition, $\gamma(t - \frac{z}{v_g^{sp}})$ represent the pulse travelling with group velocity v_g^{sp}. The pulse width is given by

$$\Gamma = \frac{\epsilon_0 \omega n_{sp}^{(0)} n_2^{sp}}{2} \tag{16}$$

The linear refractive index without Kerr field is formulated as:

$$n_{sp}^{(0)} = \sqrt{\frac{(1 + 2\pi\chi^{(0)})\,\varepsilon_c}{1 + 2\pi\chi^{(0)} + \varepsilon_c}} \tag{17}$$

The nonlinear refractive index contributed by Kerr effect is written as:

$$n_2^{sp} = \frac{2\pi F\left(1 + 2\pi\chi^{(0)} + \varepsilon_c\right)\varepsilon_c - 2\pi F\left(1 + 2\pi\chi^{(0)}\right)\varepsilon_c}{\left[1 + 2\pi\chi^{(0)} + \varepsilon_c\right]^2} \tag{18}$$

where $g = -\beta\gamma^2/2$, $\beta = 1/(v_g^{sp})^2$, $F = \partial\chi/\partial I|_{I=0}$ and $I = |\Omega_c|^2$ and $\chi^{(0)}$ is susceptibility without intensity I or Kerr field Ω_c.

Results and discussions

This study presents the outcomes of coherent control over the spatio-temporal soliton output pulse and the intensity of surface plasmon polaritons (SPPs) at the interface between a silver-silica nano-composite and a gain-assisted medium, as functions of the normalized time t/τ_0 and normalized propagation distance z/λ. The decay rate is used as $\gamma = 2\pi$ GHz and other frequency parameters are related to γ. Atomic units are used through out this works. Further $\omega = 10^3\gamma$, $k_0 = 2\pi/\lambda$, $\lambda = 2\pi c/\omega$, $\varepsilon_\infty = 6$, $\varepsilon_d = 2.25$, $f = 10\%$, $\gamma_s = 17.94\gamma$ and plasma frequency is $1.94 \times 10^2\gamma$.

Figure 2 shows the graphs depicting the behavior of soliton pulse propagation and the associated surface plasmon polariton (SPP) wave intensity at the interface of a silver-silica nano-composite material and a gain-assisted atomic medium, plotted against the normalized spatial coordinate z/λ and normalized time t/τ_0. Here, λ stands for the free-space wavelength, and τ_0 represents the duration of the pulse in the time domain. The plasmon polariton pulse $S_{sp}(z,t)$ and intensity $I_{sp}(z,t) = |S_{sp}(z,t)|^2$ are plotted in the position and time ranges of $-\lambda \le z \le \lambda$ and $0\tau_0 \le t \le 3\tau_0$ at the parameters $\Delta_p = 0.2\gamma$, $R_1 = 3.5\gamma$, $R_c = 4\gamma$, $\Delta_1 = 5\gamma$. The nonlinearity is larger with z-axis and constant value with forward time flowing. Larger nonlinearity occur at position region of $-0.2\lambda \le z \le 0.2\lambda$ where alternate dark and bright plasmon polariton soliton is investigated which fluctuated with forward time flowing. The stable solitonic pulse propagation is obtained by the cancellation of dispersion and nonlinearity. At $z = 0\lambda$ bright soliton SPPs soliton is control around which two dark solitons

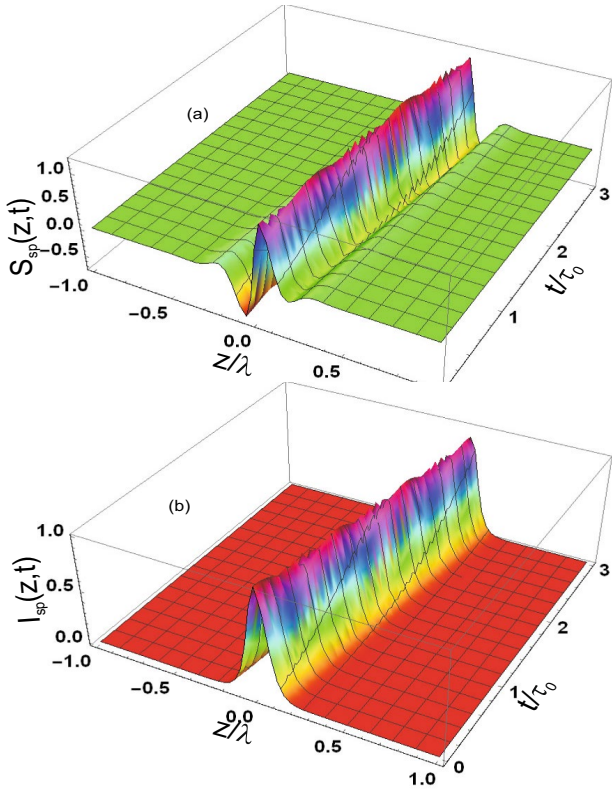

Fig. 2. The output pulse and intensity of surface plasmon polariton at interface of silver silica nano-composites material and gain assisted medium versus t/τ_0 and z/λ. The proposed parameters are $\gamma_{34,24,14} = 2.05\gamma$, $\gamma_{12} = 0.05\gamma$, $\Delta_p = 0.2\gamma$, $R_1 = 3.5\gamma$, $R_c = 4\gamma$, $\tau_0 = 1/\gamma$, $\Delta_1 = 5\gamma$.

behaviors are exist on the left and right sides. The left dark soliton behavior is decreases and right side dark soliton behavior increases with increasing time t/τ_0. The bright soliton behavior is also slowly increase with forward time growing as shown in Fig. 2a. The Solitons pulse intensity of SPPs at the interface is maximum of 100% in the position range of $-0.2\lambda \leq z \leq 0.2\lambda$ and constant with forward time flowing. The intensity is zero in other region $z \geq \pm 0.2\lambda$ and the maxima of intensity is slowly shifted to positive position with forward time increasing as demonstrated in Fig. 2b.

The results are displayed for the spatio-temporal propagation of bright and dark soliton pulses,as well as the intensity of the SPP waves at the interface between the material of silver-silica nano-composites and the gain-assisted atomic medium, as shown in Fig. 3 as a function of position z/λ and time t/τ_0 using additional parameters. The surface plasmon polariton pulse $S_{sp}(z,t)$ and intensity $I_{sp}(z,t) = |S_{sp}(z,t)|^2$ are plotted in the position and time ranges of $-\lambda \leq z \leq \lambda$ and $0\tau_0 \leq t \leq 1\tau_0$ at the parameters $\Delta_p = 0.5\gamma$, $R_1 = 3.5\gamma$, $R_c = 4\gamma$, $\tau_0 = 1/\gamma$, $\Delta_1 = 5\gamma$. Again the nonlinearity is larger with z-axis and varies with with forward time flowing. Larger nonlinearity occur at position region of $-0.3\lambda \leq z \leq 0.3\lambda$ where alternate spatio-temporal dark and bright surface plasmon polariton soliton is investigated, which fluctuated and shifted to positive position with forward time flowing. The stability is obtained due balancing of Kerr nonlinearity and dispersive effects. At $z = 0\lambda$ bright soliton of SPPs soliton is controlled around which two dark soliton behaviors exist on the left and right sides. The left dark soliton behavior decreases and right side dark soliton behavior increases with increasing time t/τ_0 and shifted to positive domain of position. The bright soliton fluctuates and shifts to positive position with forward time flowing as shown by Fig. 3a. The solitonic pulse intensity of SPPs at the interface is initial zero and become maximum, 100% in the position range of $-0.1\lambda \leq z \leq 0.1\lambda$ and with forward time growing. The intensity is zero in other region $z \geq \pm 0.2\lambda$ and the maxima of intensity is shifted to positive position with forward time as displayed in Fig. 3b.

The bright soliton pulse propagation and intensity of the SPP waves at the interface of silver-silica nano-composites material and gain assisted atomic medium are plotted against position z/λ and time t/τ_0 in Fig. 4. The parameters used are $\Delta_p = -5\gamma$, $R_1 = 2\gamma$, $R_c = 15\gamma$, and $\Delta_1 = 5\gamma$. The SPP pulse $S_{sp}(z,t)$ and intensity $I_{sp}(z,t) = |S_{sp}(z,t)|^2$ are plotted in the position and time ranges of $-\lambda \leq z \leq \lambda$ and $0\tau_0 \leq t \leq 1\tau_0$. Again the nonlinearity is larger with z-axis and constant with forward time increasing. The larger nonlinearity occur at position region of $-0.1\lambda \leq z \leq 0.1\lambda$, and bright spatio-temporal SPP soliton is controlled by balancing of dispersion and Kerr nonlinearity with forward time t/τ_0. The bright spatio-temporal soliton is constant in the position range of $-0.1\lambda \leq z \leq 0.1\lambda$ over all the time as shown in Fig. 4a. The spatio-temporal bright soliton pulse intensity of SPPs at the interface is constant with the value of 60% in the position range of $-0.1\lambda \leq z \leq 0.1\lambda$ with forward time growing as illustrated in Fig. 4b.

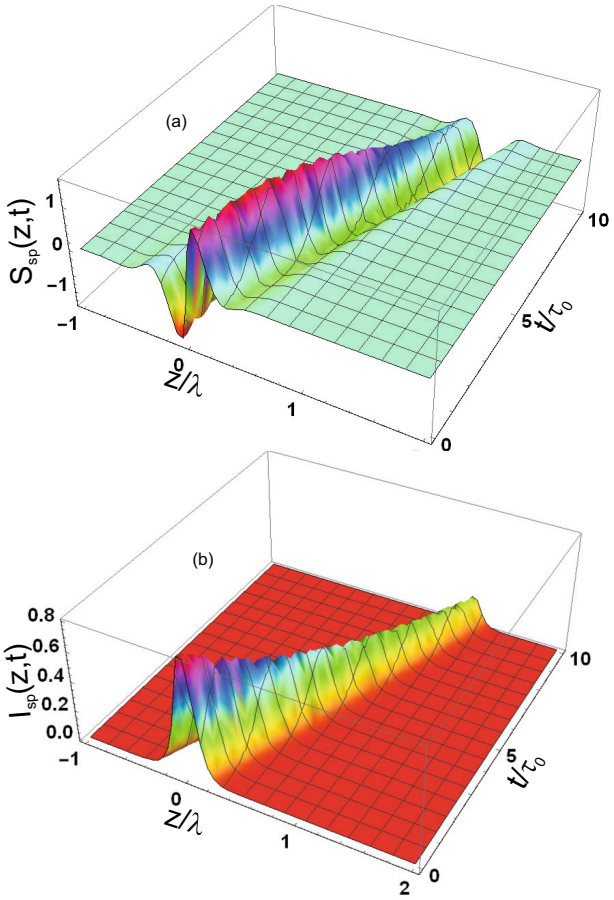

Fig. 3. The output pulse and intensity of surface plasmon polariton at interface of silver silica nano-composites material and gain assisted medium versus t/τ_0 and z/λ. The proposed parameters are $\gamma_{34,24,14} = 2.05\gamma$, $\gamma_{12} = 0.05\gamma$, $\Delta_p = 0.5\gamma$, $R_1 = 3.5\gamma$, $R_c = 4\gamma$, $\tau_0 = 1/\gamma$, $\Delta_1 = 5\gamma$.

Figure 5 shows the plots of bright and dark soliton pulse propagation along with the intensity of SPP waves at the interface between silver-silica nano-composites and gain-assisted media, presented as functions of normalized position (z/λ) and normalized time (t/τ_0). These results are obtained using the parameters $\Delta_p = 10\gamma, R_1 = 5\gamma, R_c = 3\gamma, \tau_0 = 1/\gamma$, and $\Delta_1 = -10\gamma$. The surface plasmon polariton pulse $S_{sp}(z,t)$ and intensity $I_{sp}(z,t) = |S_{sp}(z,t)|^2$ are plotted in the position and time ranges of $-\lambda \leq z \leq \lambda$ and $0\tau_0 \leq t \leq 3\tau_0$. The nonlinearity is larger with z-axis and increasing with forward time growing. The larger nonlinearity occur at position region of $-0.1\lambda \leq z \leq 0.1\lambda$, where single bright and dark spatio-temporal surface plasmon polariton soliton is controlled by balancing of dispersion and Kerr nonlinearity with forward time t/τ_0. The bright and dark spatio-temporal soliton is increasing in amplitudes in the position range of $-0.1\lambda \leq z \leq 0.1\lambda$ with the increasing of time as shown in Fig 5a. The spatio-temporal bright and dark soliton pulse intensity of SPPs at the interface is increasing with time and reach to 100% in the position range of $-0.1\lambda \leq z \leq 0.1\lambda$ with forward at $t = 3\tau_0$ as presented in Fig. 5b.

In Fig. 6 the plots are depicted again using the parameters, $\Delta_p = 0.1\gamma, R_1 = 1\gamma, R_c = 1\gamma, \Delta_1 = -0.1\gamma$. The surface plasmon polariton pulse $S_{sp}(z,t)$ and intensity $I_{sp}(z,t) = |S_{sp}(z,t)|^2$ are plotted in the position and time ranges of $-\lambda \leq z \leq \lambda$ and $0\tau_0 \leq t \leq 3\tau_0$. The larger nonlinearity occur at position region of $-0.3\lambda \leq z \leq 0.3\lambda$, where single bright and dark spatio temporal surface plasmon polariton soliton is controlled by balancing of dispersion and Kerr nonlinearity with forward time t/τ_0. The bright and dark spatio-temporal soliton is slowly decreasing in amplitudes in the position range of $-0.3\lambda \leq z \leq 0.3\lambda$ with the increasing of time as shown in Fig. 6a. The spatio-temporal bright and dark soliton pulse intensity of SPPs at the interface is decreasing with time and reach to 0% in the position range of $-0.3\lambda \leq z \leq 0.3\lambda$ with forward at $t = 4\tau_0$ as displayed in Fig. 6b.

The periodic bright and dark soliton pulse propagation and intensity of the SPP waves at the interface of silver-silica nano-composites and gain assisted media are plotted against position z/λ and time t/τ_0 in Fig. 7. The parameters used are $\Delta_p = -20\gamma$, $R_1 = 15\gamma$, $R_c = 20\gamma$, $\tau_0 = 1/\gamma$, and $\Delta_1 = 20\gamma$. The SPP pulse $S_{sp}(z,t)$ and intensity $I_{sp}(z,t) = |S_{sp}(z,t)|^2$ are plotted in the position and time ranges of $-\lambda \leq z \leq \lambda$ and $0\tau_0 \leq t \leq 0.8\tau_0$. The nonlinearity is smaller both space and time. Periodic spatio-temporal dark and bright solitons are controlled at position region of $-1\lambda \leq z \leq 1\lambda$ of surface plasmon polariton by balancing of dispersion and Kerr nonlinearity with forward time t/τ_0. The bright and dark spatio-temporal soliton is

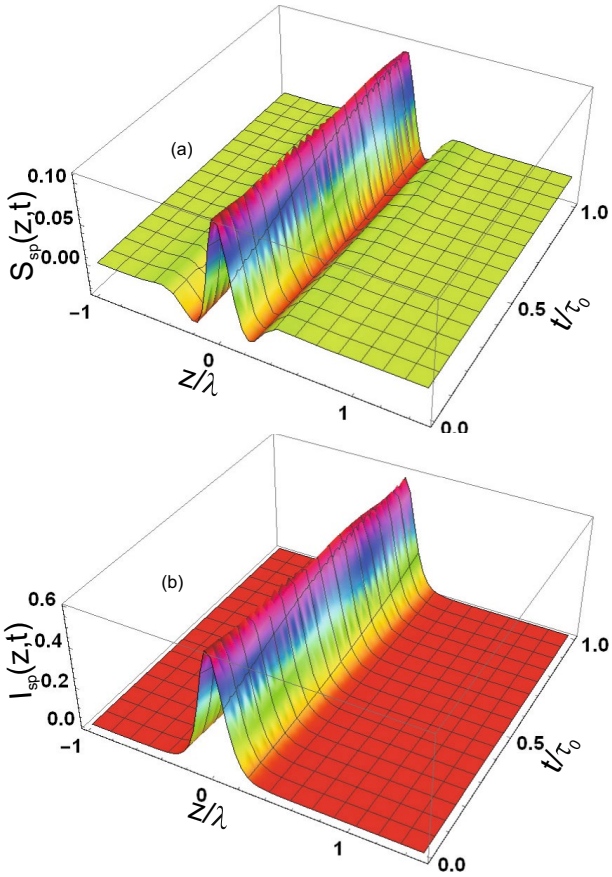

Fig. 4. The output pulse and intensity of surface plasmon polariton at interface of silver silica nano-composites material and gain assisted medium versus t/τ_0 and z/λ. The proposed parameters are $\gamma_{34,24,14} = 2.05\gamma$, $\gamma_{12} = 0.05\gamma$, $\Delta_p = -5\gamma$, $R_1 = 2\gamma$, $R_c = 15\gamma$, $\tau_0 = 1/\gamma$, $\Delta_1 = 5\gamma$.

oscillating in amplitudes in the position range of $-1\lambda \leq z \leq 1\lambda$ with the increasing of time as shown in Fig. 7a. The spatio-temporal bright and dark soliton pulse intensity of SPPs at the interface is decreasing with time and vanished in the position range of $-1\lambda \leq z \leq 1\lambda$ with forward at $t = \tau_0$ as shown in Fig. 7b.

Conclusions

The interface between the gain-assisted atomic medium and the silver silica nano-composite material was analyzed for the formation of bright and dark surface plasmon polariton (SPP) solitons. The combined dielectric response of the gain medium and the nano-composite determines the dispersion relation of SPPs, which governs their wavelength, velocity, damping, propagation, and penetration lengths. Under appropriate phase-matching conditions between the plasmon and photon modes, solitary SPP waves are generated. The coherent manipulation of spatio-temporal SPP soliton pulses at this interface has been thoroughly investigated. Alternating dark and bright plasmonic solitons were observed, exhibiting temporal oscillations. Stable soliton propagation occurs when the effects of dispersion and nonlinearity are balanced. The intensity and position of bright and dark SPP solitons can be effectively controlled by tuning the spatial coordinate, time, and driving-field parameters. The solitonic pulse intensity may increase, decrease, or remain constant with time depending on the chosen parameters. Periodic bright and dark solitons were also observed, with their intensity following an exponentially decaying trend. The intensity of SPPs varies within the range $0 \leq I_{sp} \leq 100\%$ and can be modulated through external field parameters. In specific regimes, the bright-soliton intensity increases up to 100% while in others it decays from 60 to 0%. At the exact balance of dispersion and Kerr nonlinearity, the intensity remains constant at approximately 60%, indicating stable soliton formation. The maximum soliton intensity shifts along the positive or negative z-axis over time, reflecting the nonlinear field distribution along the interface. Stability is attained in gain areas where Kerr nonlinearity counteracts dispersion. Additionally, kink and anti-kink soliton patterns were found, confined inside certain control-field detuning regions. A luminous temporal soliton was also seen, becoming more localised under significant detuning and exhibiting a gradual decline over time. This study offers a fundamental theoretical framework for understanding and controlling SPP soliton dynamics, rather than serving as a direct blueprint for immediate device fabrication. The findings illustrate the viability of manipulating plasmonic solitons via coherent gain field interactions, presenting potential applications in electrochemical sensing, biomedicine, nano-scale imaging, signal processing, logic devices, and optical switching.

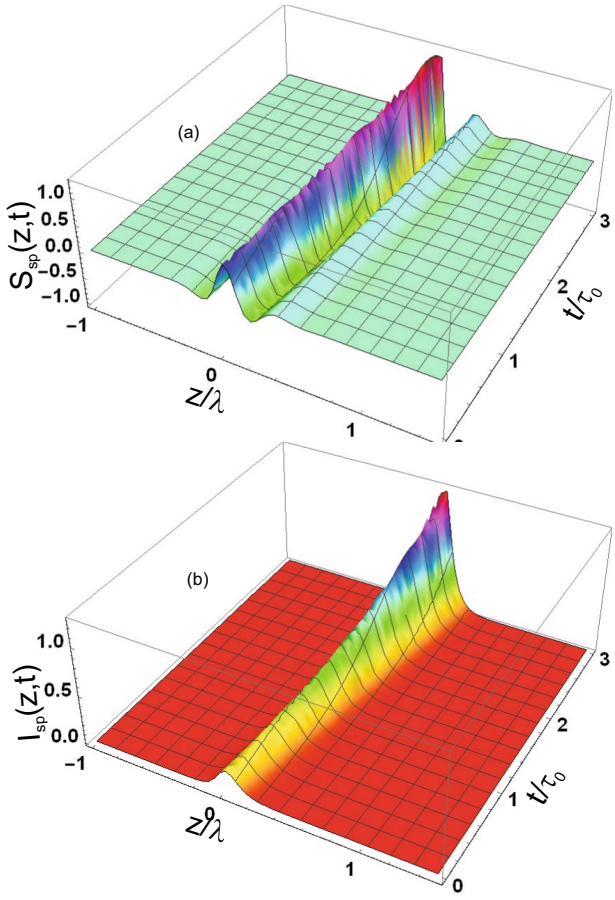

Fig. 5. The output pulse and intensity of surface plasmon polariton at interface of silver silica nano-composites material and gain assisted medium versus t/τ_0 and z/λ. The proposed parameters are $\gamma_{34,24,14} = 2.05\gamma$, $\gamma_{12} = 0.05\gamma$, $\Delta_p = 10\gamma$, $R_1 = 5\gamma$, $R_c = 3\gamma$, $\tau_0 = 1/\gamma$, $\Delta_1 = -10\gamma$.

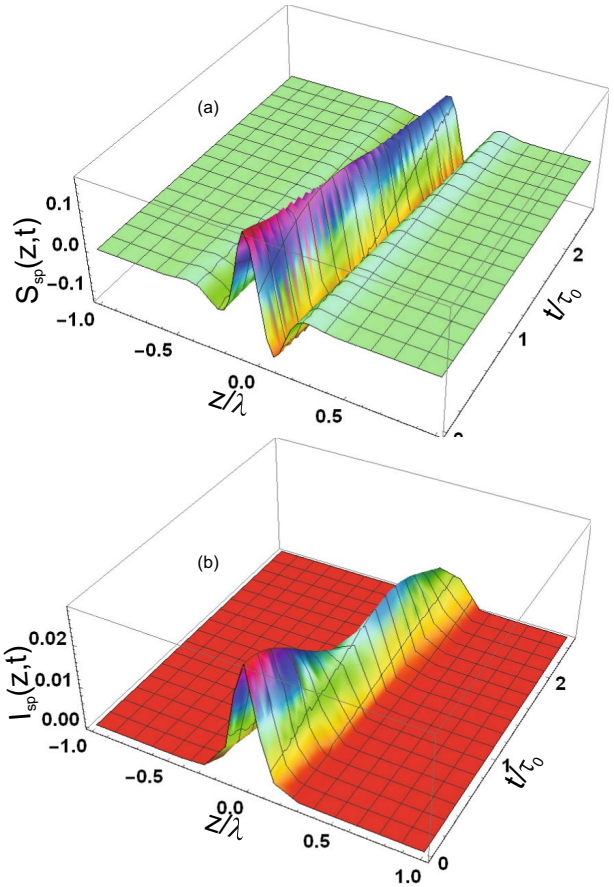

Fig. 6. The output pulse and intensity of surface plasmon polariton at interface of silver silica nano-composites material and gain assisted medium versus t/τ_0 and z/λ. The proposed parameters are $\gamma_{34,24,14} = 1.05\gamma$, $\gamma_{12} = 0.05\gamma$, $\Delta_p = 0.1\gamma$, $R_1 = 1\gamma$, $R_c = 1\gamma$, $\tau_0 = 1/\gamma$, $\Delta_1 = -0.1\gamma$.

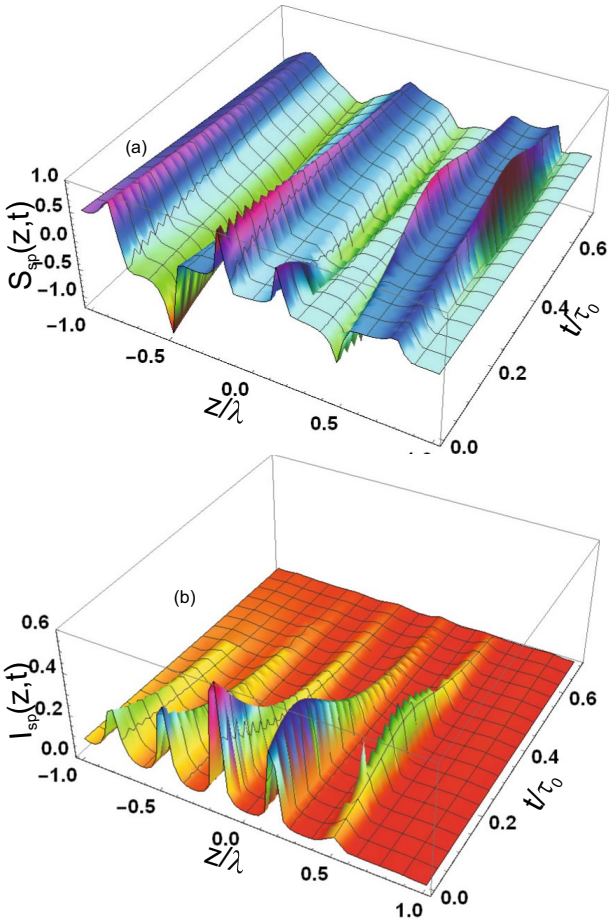

Fig. 7. The output pulse and intensity of surface plasmon polariton at interface of silver silica nano-composites material and gain assisted medium versus t/τ_0 and z/λ. The proposed parameters are $\gamma_{34,24,14} = 0.5\gamma$, $\gamma_{12} = 0.05\gamma$, $\Delta_p = -20\gamma$, $R_1 = 15\gamma$, $R_c = 20\gamma$, $\tau_0 = 1/\gamma$, $\Delta_1 = 20\gamma$.

Data availability

All data generated or analysed during this study are included in this published article, [and its supplementary information files].

Received: 13 January 2026; Accepted: 9 April 2026
Published online: 20 April 2026

References

1. Yi, X., Yang, Q. F., Yang, K. Y. & Vahala, K. Imaging soliton dynamics in optical microcavities. *Nat. Commun.* **9**(1), 3565 (2018).
2. Denschlag, J. et al. Generating solitons by phase engineering of a Bose–Einstein condensate. *Science* **287**(5450), 97–101 (2000).
3. Mollenauer, L. F., Stolen, R. H. & Gordon, J. P. Experimental observation of picosecond pulse narrowing and solitons in optical fibers. *Phys. Rev. Lett.* **45**(13), 1095 (1980).
4. Yang, Y. *Solitons in Field Theory and Nonlinear Analysis* (Springer, 2001).
5. Hu, X. et al. Novel optical soliton molecules formed in a fiber laser with near-zero net cavity dispersion. *Light Sci. Appl.* **12**(1), 38 (2023).
6. Wang, Y. et al. Vector soliton generation in a Tm fiber laser. *IEEE Photon. Technol. Lett.* **26**, 769–72 (2014).
7. Sun, Z. Y., Gao, Y. T., Yu, X. W., Liu, J. & Liu, Y. Bound vector solitons and soliton complexes for the coupled nonlinear Schrodinger equations. *Phys. Rev. E* **80**(9), 066608–066617 (2009).
8. Cui, Y., Zhang, Y., Huang, L. & Liu, X. Dual-state vector soliton in mode-locked fiber laser. *Opt. Laser Technol.* **157**, 108674 (2023).
9. Ackemann, T., Firth, W. & Oppo, G. L. Fundamentals and applications of spatial dissipative solitons in photonic devices. *Adv. At. Mol. Opt. Phys.* **57**, 323–421 (2009).
10. Kivshar, Y. S. & Agrawal, G. P. *Optical Solitons: from Fibers to Photonic Crystals* (Academic Press, 2003).
11. Ferreira, A. C. et al. Analysis of the nonlinear optical switching in a Sagnac interferometer with non-instantaneous Kerr effect. *Opt. Commun.* **285**(6), 1408–17 (2012).
12. Zhang, H., Tang, D. Y., Zhao, L. N. & Xiang, N. Coherent energy exchange between components of a vector soliton in fiber lasers. *Opt. Express* **16**(5), 12618–23 (2008).
13. Yang, J. Interaction of two vectors solitons. *Phys. Rev. E* **64**(12), 026607–026619 (2001).
14. Kaup, M. J. Imternal dynomics of a vectors solitons in a nonlinear optical fiber. *Am. Phys. Soc.* **48**(1), 3049–53 (1993).
15. Dumitru, M., Mazilu, D. & Torner, L. Stability of walking vector solitons. *Phy. Rev. Lett.* **81**, 453–455 (1998).

16. Song, Y. F., Li, L., Zhang, H., Shen, D. Y. & Loh, K. P. Vector multi-soliton operation and interaction in a graphene mode-locked fiber laser. *Opt. Express* **21**, 10010 (2013).
17. Lu, F., Lin, Q., Knox, W. H. & Agarwal, G. P. Vector soliton fission. *Phys. Rev. Lett.* **93**, 183901 (2004).
18. Kbashi, H. J., Sergeyev, S. V., Araimi, M. A., Tarasov, N. & Rozhin, A. Vector soliton rain. *Laser Phys. Lett.* **16**, 035103 (2019).
19. Ye, R., Zhang, Y. & Xiu, W. M. Partial differential equations in applied mathematics. *Light Appl. Math.* **4**, 100161 (2021).
20. Zhu, Z., Yang, S., He, C. & Lin, X. Vector pure-quartic soliton molecule fiber laser. *Chaos Solitons Fractals* **175**, 113978 (2023).
21. Ding, C., Gao, Y., Hu, L., Deng, G. & Zhang, C. Vector bright soliton interactions of the two-component AB system in a baroclinic fluid. *Chaos Solitons Fractals* **142**, 110363 (2021).
22. Xu, T. F., Li, W. L., Li, Z. & Zhang, C. Phase diagram and dynamics of dark-bright vector solitons in spin–orbit-coupled Bose–Einstein condensate. *Chaos Solitons Fractals* **111**, 62–7 (2018).
23. Tang, Q., Zhang, Y., Kartashov, Y. V., Li, Y. & Konotop, V. V. Vector valley hall edge solitons in superhoneycomb lattices. *Chaos Solitons Fractals* **161**, 112364 (2022).
24. Djazet, A., Fewo, S. I., Djoko, M., Felenou, E. T. & Kofane, T. C. Extension of the stability criterion for dissipative vector solitons of a laser coupled two-dimensional Ginzburg–Landau equation generated from vector asymmetric inputs. *Chaos Solitons Fractals* **170**, 113390 (2023).
25. Huang, K. et al. Quantum squeezing of vector slow-light solitons in a coherent atomic system. *Chaos Solitons Fractals* **163**, 112557 (2022).
26. Tang, D. Y., Zhang, H., Zhao, L. M. & Wu, X. Observation of high-order polarizationlocked vector solitons in a fiber laser. *Phys. Rev. Lett.* **101**(15), 153904 (2008).
27. Li, Z. et al. Ultrashort dissipative Raman solitons in Kerr resonators driven with phase-coherent optical pulses. *Nat. Photon.* **18**, 1–8 (2023).
28. Jang, J. K., Erkintalo, M., Murdoch, S. G. & Coen, S. Ultraweak long-range interactions of solitons observed over astronomical distances. *Nat. Photon.* **7**(8), 657–63 (2013).
29. Obrzud, E., Lecomte, S. & Herr, T. Temporal solitons in microresonators driven by optical pulses. *Nat. Photon.* **11**(9), 600–7 (2017).
30. Xue, X. et al. Dispersion-less Kerr solitons in spectrally confined optical cavities. *Light Sci. Appl.* **12**(1), 19 (2023).
31. Melnikov, I. V., Papageorgakis, C. & Royston, A. B. Forced soliton equation and semiclassical soliton form factors. *Phys. Rev. Lett.* **125**(23), 231601 (2020).
32. Averlant, E., Tlidi, M., Panajotov, K. & Weicker, L. Coexistence of cavity solitons with different polarization states and different power peaks in all-fiber resonators. *Opt. Lett.* **42**, 2750 (2017).
33. Huang, T. et al. Coexistence of nonlinear states with different polarizations in a Kerr resonator. *Phys. Rev. A* **109**, 013503 (2024).
34. Amdad, Chowdury, Wonkeun, Chang & Marco, Battiato. Higher-order rogue-wave fission in the presence of self-steepening and Raman self-frequency shift. *Phys. Rev. A* **107**(5), 053507 (2023).
35. Rehman, K. U., Shatanawi, W., Bahaidarah, H. M. S., Abbas, S. & Khan, A. U. Thermal case study of nanofluid flow in partially heated rectangular enclosure rooted with sinusoidal heated rods and inclined magnetic field. *Case Stud. Therm. Eng.* **45**, 102982 (2023).
36. Rehman, K. U. & Shatanawi, W. Thermal analysis on mutual interaction of temperature stratification and solutal stratification in the presence of non-linear thermal radiations. *Case Stud. Therm. Eng.* **35**, 102080 (2022).
37. Rehman, K. U., Shatanawi, W. & Shatnawi, T. A. Machine learning based analysis of heat transfer in tangent hyperbolic fluid at heat generating magnetized surface. *Int. J. Thermofluids* **21**, 100573 (2024).
38. Kostet, B., Soupart, Y., Panajotov, K. & Tlidi, M. Coexistence of dark vector soliton Kerr combs in normal dispersion resonators. *Phys. Rev. A* **104**(5), 053530 (2021).
39. Nielsen, A. U., Garbin, B., Coen, S., Murdoch, S. G. & Erkintalo, M. Coexistence and interactions between nonlinear states with different polarizations in a monochromatically driven passive Kerr resonator. *Phys. Rev. Lett.* **123**(1), 013902 (2019).
40. Ozbay, E. Plasmonics: Merging photonics and electronics at nanoscale dimensions. *Science* **311**, 189–193 (2006).
41. Barnes, W. L., Dereux, A. & Ebbesen, T. W. Surface plasmon subwavelength optics. *Nature (London)* **424**, 824 (2003).
42. Vasa, P. & Lienau, C. Strong light-matter interaction in quantum emitter/metal hybrid nanostructures. *ACS Photon.* **5**, 2–23 (2018).
43. Chen, K. Y., Janz, K. F., Zhu, W. & Brychta, R. J. Re-defining the roles of sensors in objective physical activity monitoring. *Med. Sci. Sports Exerc.* **44**, S13 (2012).
44. Bernardi, M. et al. Theory and computation of hot carriers generated by surface plasmon polaritons in noble metals. *Nat. Commun.* **6**, 7044. https://doi.org/10.1038/ncomms8044 (2015).
45. Zhang, Z., Fang, Y., Wang, W., Chen, L. & Sun, M. Propagating surface plasmon polaritons: Towards applications for remoteexcitation surface catalytic reactions. *Adv. Sci.* **3**, 1500215. https://doi.org/10.1002/advs.201500215 (2016).
46. Tame, M. et al. Quantum plasmonics. *Nat. Phys.* **9**, 329–340. https://doi.org/10.1038/nphys2615 (2013).
47. Fitzgerald, J. M., Narang, P., Craster, R. V., Maier, S. A. & Giannini, V. Quantum Plasmonics. *Proc. IEEE* **104**(12), 2307–2322 (2016).
48. Dragoman, M. & Dragoman, D. Plasmonics: Applications to nanoscale terahertz and optical devices. *Prog. Quant. Electron.* **32**(1), 1–41 (2008).
49. Claridge, S. A., Liang, H. W., Basu, S. R., Frsechet, J. M. & Alivisatos, A. P. Isolation of discrete nanoparticle-DNA conjugates for plasmonic applications. *Nano Lett.* **8**(4), 1202–1206 (2008).
50. Jain, P. K., Huang, X., El-Sayed, I. H. & El-Sayed, M. A. Noble metals on the nanoscale: Optical and photothermal properties and some applications in imaging, sensing, biology, and medicine. *Acc. Chem. Res.* **41**(12), 1578–1586 (2008).
51. Wang, H. et al. Sensitivity-enhanced surface plasmon resonance sensor utilizing a tungsten disulfide (WS2) nanosheets overlayer. *Photon. Res.* **6**(6), 485–491 (2018).
52. Farmani, A., Jafari, M. & Miremadi, S. S. A high performance hardware implementation image encryption with AES algorithm. In *Third International Conference on Digital Image Processing (ICDIP 2011)*, vol. 8009, 800905 (International Society for Optics and Photonics, 2011).
53. Farmani, A., Zarifkar, A., Sheikhi, M. H. & Miri, M. Design of a tunable graphene plasmonic-on-white graphene switch at infrared range. *Superlattices Microstruct.* **112**, 404–414 (2017).
54. Maji, P. S., Shukla, M. K. & Das, R. Blood component detection based on miniaturized self-referenced hybrid Tamm-plasmonpolariton sensor. *Sens. Actuators B Chem.* **255**, 729–734 (2018).
55. Akbari, E. et al. Silicene and graphene nano materials in gas sensing mechanism. *RSC Adv.* **6**(85), 81647–81653 (2016).
56. Islam, M. N. et al. Optical biosensing strategies for DNA methylation analysis. *Biosens. Bioelectron.* **92**, 668–678 (2017).
57. Maji, P. S. & Das, R. Hybrid-Tamm-plasmon-polariton based selfreference temperature sensor. *J. Light Technol.* **35**(14), 2833–2839 (2017).
58. Shahrokhian, S., Ghalkhani, M., Adeli, M. & Amini, M. K. Multiwalled carbon nanotubes with immobilised cobalt nanoparticle for modification of glassy carbon electrode: Application to sensitive voltammetric determination of thioridazine. *Biosens. Bioelectron.* **24**(11), 3235–3241 (2009).
59. Khozeymeh, F. & Razaghi, M. Cylindrical optical resonators: Fundamental properties and bio-sensing characteristics. *J. Opt.* **20**(4), 045301 (2018).
60. Sun, S., Chen, H. T., Zheng, W. J. & Guo, G. Y. Dispersion relation, propagation length and mode conversion of surface plasmon polaritons in silver double-nanowire systems. *Opt. Express* **21**, 14591–14605 (2013).

61. Asgarnezhad-Zorgabad, S., Sadighi-Bonabi, R. & Sanders, B. C. Excitation and propagation of surface polaritonic rogue waves and breathers. *Phys. Rev. A* **98**, 013825 (2018).
62. Asgarnezhad-Zorgabad, S., Sadighi-Bonabi, R. & Hang, C. Coupler-free surface polariton excitation and propagation with cold four-level atomic medium. *J. Opt. Soc. Am. B* **34**, 1787–1795 (2017).
63. Asgarnezhad-Zorgabad, S., Sadighi-Bonabi, R., Kibler, B., Zdemir, S. K. & Sanders, B. C. Surface-polaritonic phase singularities and multimode polaritonic frequency combs via dark rogue-wave excitation in hybrid plasmonic waveguide. *Netw. J. Phys.* **22**, 033008 (2020).
64. Tan, C. & Huang, G. Surface polaritons in a negative-index metamaterial with active Raman gain. *Phys. Rev. A* **91**, 023803 (2015).
65. Khan, S., Saeed, M., Khan, M. A., Aldosary, S. F. & Ahmad, S. Coherent manipulation of optical soliton in four-level N-type atomic medium. *Int. J. Theor. Phys.* **63**, 181 (2024).
66. Agarwal, G. S. & Dasgupta, S. Superluminal propagation via coherent manipulation of the Raman gain process. *Phys. Rev. A* **70**, 023802 (2004).
67. Ullah, S., Wahid, U., Bacha, B. A., Ullah, A. & Ullah, Z. Particle microscopy by surface plasmon polariton waves at the interface of dielectric and silver silica nano-composites. *Phys. Scr.* **96**, 01510 (2020).
68. Dey, T. N. & Agarwal, G. S. Observable effects of Kerr nonlinearity on slow light. *Phys. Rev. A* **76**, 015802 (2007).

Acknowledgements
Authors are thankful to Prince Sultan University for APC and support through TAS research lab.

Author contributions
Naseem Elahi: Wrote the original manuscript, conceptualization, investigation, writing review, and editing. Muhammad Ikram: Software, supervision, methodology. Najm uddin: Software, calculation, data curation, writing review, and editing. Latif Ur Rahman: Software, calculation, writing review, and editing. Nahid Fatima: Resources, and funding acquisition. Kamal Shah: Formal analysis, resources, calculations, and funding acquisition. Thabet Abdeljawad: Data curation, resources, and funding acquisition.

Declarations

Competing interests
The authors declare no competing interests.

Additional information
Correspondence and requests for materials should be addressed to M.I., L.U.R. or T.A.

Reprints and permissions information is available at www.nature.com/reprints.

Publisher's note Springer Nature remains neutral with regard to jurisdictional claims in published maps and institutional affiliations.